Biol. Cybern. 84, 123–132 (2001)

Biological Cybernetics

Hippocampal rhythm generation: Gamma-related theta-frequency resonance in CA3 interneurons

G. Orbán, T. Kiss, M. Lengyel, P. Érdi

Department of Biophysics, KFKI Research Institute for Particle and Nuclear Physics, Hungarian Academy of Sciences, P.O. Box 49, 1525 Budapest, Hungary

Received: 23 February 2000 / Accepted in revised form: 30 June 2000

Abstract. During different behavioral states different population activities are present in the hippocampal formation. These activities are not independent: sharp waves often occur together with high-frequency ripples, and gamma-frequency activity is usually superimposed on theta oscillations. There is both experimental and theoretical evidence supporting the notion that gamma oscillation is generated intrahippocampally, but there is no generally accepted view about the origin of theta waves. Precise timing of population bursts of pyramidal cells may be due to a synchronized external drive. Membrane potential oscillations recorded in the septum are unlikely to fulfill this purpose because they are not coherent enough. We investigated the prospects of an intrahippocampal mechanism supplying pyramidal cells with theta frequency periodic inhibition, by studying a model of a network of hippocampal inhibitory interneurons. As shown previously, interneurons are capable of generating synchronized gamma-frequency action potential oscillations. Exciting the neurons by periodic current injection, the system could either be entrained in an oscillation with the frequency of the inducing current or exhibit in-phase periodic changes at the frequency of single cell (and network) activity. Simulations that used spatially inhomogeneous stimulus currents showed anti-phase frequency changes across cells, which resulted in a periodic decrease in the synchrony of the network. As this periodic change in synchrony occurred in the theta frequency range, our network should be able to exhibit the theta-frequency weakening of inhibition of pyramidal cells, thus offering a possible mechanism for intrahippocampal theta generation.

1 Introduction

Global brain states, under both normal and pathological conditions, may be associated with spontaneous rhythmic activities of large populations of neurons. Experimentally, these activities may be detected by recording both from large neural assemblies (as in EEG) or from a single neuron of a cell population (Buzsáki et al. 1983; Fox and Ranck 1986). Two main, normally occurring global hippocampal states are known: rhythmic slow activity, called theta rhythm with the associated gamma oscillation; and irregular sharp waves with the associated high-frequency (ripple) oscillation. (A pathological brain state, associated with epileptic seizures, is also a common pattern in the hippocampus.) Although many data connect rhythmic brain states to behavioral correlates (Buzsáki et al. 1983; Stewart and Fox 1990) their functional significance has not yet been clarified.

Theta rhythms are thought to be involved in time-locking cell activities (Ylinen et al. 1995), time-stamping for phase coding (O'Keefe and Recce 1993), increasing the signal to noise ratio (Katona et al. 1999), and regulating cellular learning (O'Keefe and Recce 1993; Skaggs et al. 1996). Gamma oscillation is thought to play a central role (in neocortex) in binding perceived and recalled attributes of events (Gray et al. 1989), and (in hippocampus) in forming memory traces (Jensen and Lisman 1996). During irregular sharp waves, memory traces are thought to be consolidated and transferred to neocortex (Buzsáki 1998).

Theta rhythm is a population oscillation with a large amplitude (1 mV) and a frequency of 4–12 Hz. It is found to occur whenever an animal engages in walking, exploration, or sensory scanning, as well as during REM sleep (Vanderwolf 1969). Single-cell physiological studies showed different relationships between the behavior of individual cells and the theta rhythm. Pyramidal cells in the hippocampus proper generally discharge with a very low frequency (0.01–0.5 Hz), although spatially sensitive place cells show firing at 4–8 Hz when the rat is in their place fields, and the position of the animal within the place field of a cell may be correlated with the phase of its firing relative to the theta rhythm (O'Keefe and Recce 1993). Particular cell populations were shown to behave differently during the presence of theta-frequency membrane potential oscillations. While CA1 pyramidal

Correspondence to: P. Érdi

neurons and granule cells fire at the troughs of extracellularly recorded theta oscillations, action potentials of basket cells were present near the peaks (Ylinen et al. 1995). Studies assign the medial septum to be the pacemaker of the hippocampal theta (Petsche et al. 1962; Alonso and Garcia-Austt 1987), with an interplay of the entorhinal cortex (Ylinen et al. 1995). However in vitro experiments suggested that it could also be generated internally, by the intrinsic membrane properties of neurons of the CA3 region (Leung and Yim 1991; Strata 1998).

Gamma-frequency field oscillations reflect synchronized synaptic potentials in neuronal populations within an approximate 2-mm range along the longitudinal axis of the hippocampus (Bragin et al. 1995), and within a 7-mm range in the cat visual cortex. The frequency of this oscillation is 20–80 Hz. Mechanisms underlying gamma oscillations are not fully understood: previous hypotheses suggested that the origin of synchronized gamma activity may be mutual excitation among principal cells or individual chattering cells (Traub et al. 1999a). An alternative hypothesis is that – in the hippocampus – synchronized gamma oscillations are generated by an inhibitory interneuron network (Whittington et al. 1995; Wang and Buzsáki 1996; Traub et al. 1999a).

The notion of interneuron network-generated gamma oscillation is supported by numerous experimental findings. Hippocampal interneurons are intrinsically capable of producing high-frequency periodic firing, and may also show resonance at theta frequencies (Chapman and Lacaille 1999). In addition, sparsely spiny inhibitory interneurons in cortical layer IV (Wang 1993) and CA1 interneurons (Bragin et al. 1995) can sustain a 40-Hz oscillation. It may be hypothesized that inhibitory interneurons of CA3 can exhibit intrinsic 40–100 Hz oscillations due to tonic depolarization maintained by the septum (Léránth and Frotscher 1987) or the perforant path (Buzsáki et al. 1987).

An important and often observed phenomenon is the co-occurence of theta and gamma activity (Leung et al. 1982; Buzsáki et al. 1983). Physiological experiments have revealed that the amplitude of gamma oscillations is strongly modulated by theta-frequency oscillations, and long term changes of the amplitude and frequency of the two activities are positively correlated (Bragin et al. 1995). However, the mechanism responsible for generating gamma-related theta rhythm remains unclear. Our aim in this study was to find a neurobiologically plausible mechanism to explain the origin of the theta–gamma correlation.

2 Methods

The equations and parameters that define the model precisely can be found in the Appendix.

2.1 Single cells

Each interneuron can be considered as an electrotonically compact unit, therefore a single-compartment model was used (Wang and Buzsáki 1996). The membrane potential changed according to the current balance equation (A1). A leakage current term (A2) was introduced to represent the passive properties of the membrane, with a resistance of $g_L^{-1} = 1\,\Omega\mathrm{m}^2$. The equilibrium potential of the leakage current was $E_L = -65\,\mathrm{mV}$. Membrane capacitance was $C_m = 0.01\ \mathrm{F/m}^2$, giving a passive time constant of $\tau_0 = 0.01$ s.

Hodgkin–Huxley-type Na^+ and K^+ channels (Hodgkin and Huxley 1952) were used to generate action potentials (A3, A6). The reversal potentials and maximal conductances were $E_{Na} = 55\,\mathrm{mV}$ and $E_K = -90\,\mathrm{mV}$, $g_{Na} = 350\ \mathrm{S/m}^2$ and $g_K = 90\ \mathrm{S/m}^2$ for sodium and potassium, respectively. Activation of the sodium conductance (m) was assumed to be fast and was thus substituted by its steady-state function (A4); other activation and deactivation variables obeyed first-order kinetics (A5, A7), with $\phi = 2$. The membrane surface area was $A_m = 1.25 \times 10^{-9}\ \mathrm{m}^2$.

With these kinetics and parameters the model interneurons reproduced basic firing properties of hippocampal interneurons. Firstly, action potentials were followed by a short after-hyperpolarization period that reached about $-70\,\mathrm{mV}$ at its minimum. Secondly, stimulating these cells with a constant input current resulted in repetitive action potentials, as assumed in earlier work (Bragin et al. 1995). The firing rate could be as high as 400 Hz if current at 20 $\mu\mathrm{A/cm}^2$ was applied. The last term of (A1) is a peripheral input whose exact form is specified for each simulation class separately (see Sect. 2.3).

2.2 Network

For connecting individual cells, $GABA_A$-mediated inhibitory synapses were used. The synaptic current was of the standard form (A8) with a maximal conductance g_{syn} of $1\ \mathrm{S/m}^2$. The reversal potential for this synapse was $E_{syn} = -75\,\mathrm{mV}$. The synaptic gating also obeyed first-order kinetics (A9). The synaptic threshold, Θ_{syn} (A10), was set to a value (0 mV) that enabled inhibitory post synaptic potential (IPSP) generation only when the presynaptic cell emitted a spike. The rise time of the IPSP was 10 ms and its minimal value was about $-67\,\mathrm{mV}$ using these synaptic parameters.

Our interneuron network model consisted of $N = 50$ cells. The connection strength between two cells was equal for all pairs as we did not intend to study the effects of the spatial distribution of neurons. Symmetric connections between cells were permitted, i.e., independent from the connection from cell A to cell B, cell B could innervate cell A. In their study, Wang and Buzsáki (1996) showed that the number of synaptic connections per cell – rather than relative connectivity – has a critical role in synchronization. Their results showed that approximately 40 synaptic connections per cell were needed for emergent synchronization. This number could be lower in the case of locally random connections (Traub et al. 1999b). As the number of synaptic connections was of critical importance in our simulations,

we used full connectivity so that the number of synaptic connections was $N-1$ per cell.

2.3 Stimulus

We investigated three paradigms which differed mainly in the stimulus to the network. The first type of stimulus was a uniform constant current (characterized only by its amplitude I_{DC}) to all cells. In the second case, cells received an additional periodic (sinusoidal or square waveform) stimulus, with the same frequency (f_{input}), amplitude (I_{AC}), and phase for all cells. This gamma-band stimulus term could correspond to periodic excitation from the entorhinal cortex (Chrobak and Buzsáki 1998). In the third paradigm, the phase of the oscillatory component was chosen randomly for each cell either with uniform distribution over the 0–360° range or from a Gaussian distribution with a given standard deviation (σ_{ph}). The mean value for the distribution was not defined, since only relative phase lags had any importance. A common feature of these types of stimuli was that cells always received some amount of constant input current. This way, independent units of the network behaved as autonomous oscillators with a given frequency. The frequency of the oscillation of a neuron was determined primarily by its parameters and by the amplitude of the input current, but could also be perturbed by the network. This depolarizing injection to our model interneurons could be interpreted as afferent input coming through cholinergic fibers of the septum or through the perforant path (Léránth and Frotscher 1987).

2.4 Analysis

To get a qualitative insight into the synchronized behavior of the network we did not need the full data set (i.e., the membrane potential traces of all cells) yielded from the numerical solution of differential equations. Rather, only spiking times had to be stored from the raw data set:

$$t_i^{\mathrm{spiking}} := \left\{ t \mid V_i(t) = \Theta_{\mathrm{firing}} \wedge \dot{V}_i(t) \geq 0 \right\} \tag{1}$$

In this way the phase space was discretized so that only the firing and silent states of neurons were distinguished (Fig. 1A):

$$F_i^{\tau}(l) = \left| t_i^{\mathrm{spiking}} \cap \{ t \mid l\tau \leq t < (l+1)\tau \} \right| \tag{2}$$

with τ being the width of the time bin used for discretization, and $V_i(t)$ being the membrane potential of the ith cell ($\Theta_{\mathrm{firing}} = 0$ mV).

To reveal temporal relationships between spike trains on a raster diagram, a cross-correlation measure was defined (Wang and Buzsáki 1996):

$$\kappa_{ij}^{\tau} = \frac{\sum_{l=0}^{K-1} F_i^{\tau}(l) F_j^{\tau}(l)}{\sqrt{\sum_{l=0}^{K-1} F_i^{\tau 2}(l) \sum_{l=0}^{K-1} F_j^{\tau 2}(l)}} \quad , \tag{3}$$

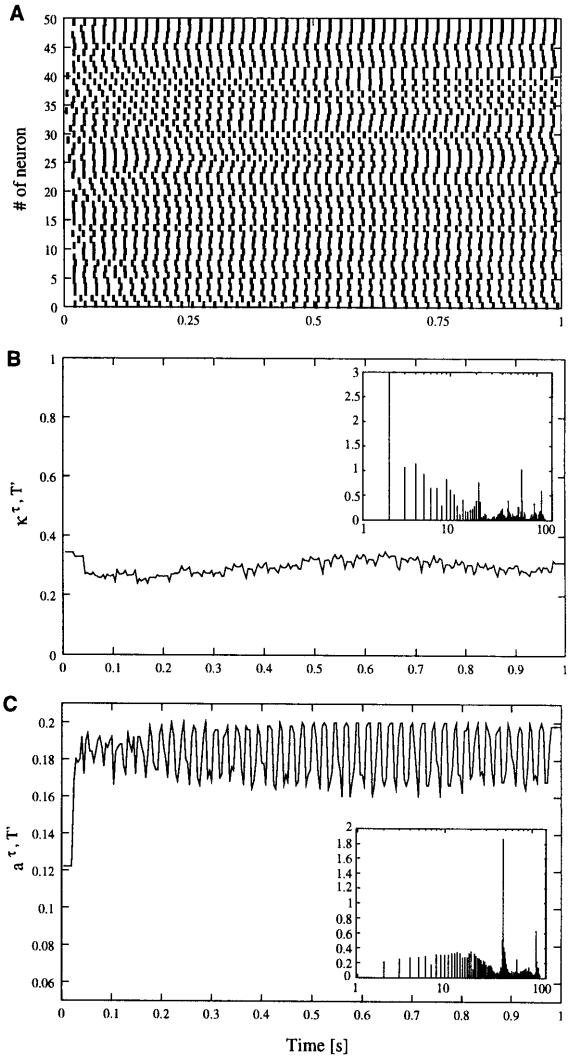

Fig. 1A–C. Characterization of network behavior. **A** Raster diagram showing binary spike trains of neurons constituting our network. Binary spike trains were discretized from spike trains generated by simulations: their value was 1 (*dark rectangles*) if a neuron fired in a time bin, and was 0 elsewhere. Horizontal axis shows time, vertical axis shows ordinal number of neurons. **B** Network correlation function $\kappa^{\tau,T'}$, acquired by calculating the cross-correlation of spike trains over all neuron pairs in a shifting time window ($T' = 40$ ms, see text). **C** Network activity $a^{\tau,T'}$ is a "spike-density" function showing the number of spikes in a shifting time window as in **B**. *Insets* in **B** and **C** show power spectra of $\kappa^{\tau,T'}$ and $a^{\tau,T'}$ respectively. All subfigures belong to the same simulation

where K is the number of time bins, computed as the quotient of the simulation time (T) and the resolution of discretization (τ).

A measure of the whole network can be obtained if we sum $\kappa_{i,j}^{\tau}$ over all neuron pairs. When it is normalized by the number of pairs ($\eta = N(N-1)/2$) its value is 1 in the fully synchronized state:

$$\kappa^{\tau} = \frac{1}{\eta} \sum_{i=2}^{N} \sum_{j=1}^{i-1} \kappa_{ij}^{\tau} \tag{4}$$

When K is not $\frac{T}{\tau}$ but $\frac{T'}{\tau}$ (where T' is an arbitrary time interval), one can define a time-dependent measure for synchronization (see Fig. 1B):

$$\kappa^{\tau,T'}(t) = \frac{1}{\eta}\sum_{i=2}^{N}\sum_{j=1}^{i-1}\frac{\sum_{l=\left[\frac{t}{\tau}\right]}^{\left[\frac{t+T'}{\tau}\right]} F_i^{\tau}(l)F_j^{\tau}(l)}{\sqrt{\sum_{l=\left[\frac{t}{\tau}\right]}^{\left[\frac{t+T'}{\tau}\right]} F_i^{\tau 2}(l)\sum_{l=\left[\frac{t}{\tau}\right]}^{\left[\frac{t+T'}{\tau}\right]} F_j^{\tau 2}(l)}} \tag{5}$$

Thus time window T' is shifted by τ, and in every window κ^{τ} has to be computed. Usually the time window is determined by the largest interspike interval. As we wanted to compare functions obtained from different simulations, we set the window size to a constant value of $T' = 40$ ms across all simulations. In experimental studies of synchronously oscillating interneuron networks (Buzsáki et al. 1992; Whittington et al. 1995), phase lags of approximately 3 ms were observable. Thus, when analysing our data we assumed two neurons to be phase locked and firing synchronously if they fired within a time interval of $\tau = 4$ ms.

Another way of recognizing certain patterns in the output of the system is to plot the activity of the network (i.e., the number of spikes) as a function of time (see Fig. 1C):

$$a^{\tau,T'}(t) = \frac{1}{N}\sum_{i=1}^{N}\sum_{l=\left[\frac{t}{\tau}\right]}^{\left[\frac{t+T'}{\tau}\right]} F_i^{\tau}(l) \tag{6}$$

where the length of the time window (T') was chosen as for $\kappa^{\tau,T'}$. Computing $a^{\tau,T'}$ requires considerably less time than computing $\kappa^{\tau,T'}$. A shortcoming of the activity function is that it can only be used to visualize the change of synchrony, since there is approximately the same number of spikes present in a time window during a steady synchronized or a steady desynchronized state. Changes in the synchrony of periodic signals can be seen only if the phases of these signals are shifting relative to each other.

The analysis of periodic processes in the network was performed in three ways. Firstly, temporal changes were described in the instantaneous frequency of individual cells. Instantaneous frequency at a given time ($f_i(t)$) is the reciprocal of the interspike interval (ISI) between the most recent and the nearest future spike:

$$\mathrm{ISI}_i(t) = \min\left(t_i^{\mathrm{spiking}} \cap \{t_2 \mid t_2 > t\}\right) - \max\left(t_i^{\mathrm{spiking}} \cap \{t_1 \mid t_1 \le t\}\right) \tag{7}$$

$$f_i(t) = \frac{1}{\mathrm{ISI}_i(t)} \tag{8}$$

Second, a normalized frequency distribution was constructed for the network from the average firing frequencies of all cells, where the average firing frequency of each cell was computed ($\overline{f_i}$) as a time average of its instantaneous firing frequency series. The average frequency of the network ($\overline{f_{\mathrm{net}}}$) was given by the mean value of this distribution. The standard error for this mean value is denoted by $\sigma_{\overline{f_{\mathrm{net}}}}$. The eigen-frequency of the network was defined as its average frequency when responding to constant current injection (first input paradigm, see Sect. 2.3).

Third, the power spectrum of network synchrony ($\kappa^{\tau,T'}$) was computed (see Fig. 1B, inset) and its weighted average around the highest peak was calculated (f_{Θ}). The same analysis could be performed for network activity ($a^{\tau,T'}$; see Fig. 1C, inset).

If, for the sake of calculating statistical significance, several simulations were run with the same parameters, frequency-distribution functions were first computed for each simulation and then averaged across simulations.

2.5 Numerical methods

Computer simulations were performed on Linux-platform PCs (kernel version 2.0.34) with AMD K6/2 300 MHz and Intel Pentium 166 MHz processors, using the GENESIS software package (version 2.1). The forward Euler numerical integration scheme was used with a time step τ_{sim} of 10^{-5} s. The simulation time (T) was 0.5–2 s. Off-line data analysis was performed using Octave (version 2.0.13), on the same platform.

3 Results

3.1 Spatially homogeneous time-independent stimulating current

To reveal basic firing properties of the model neurons all of them were stimulated by the same current generator producing a constant input current (see also Sect. 2.3). Using this stimulus, both single-cell properties (i.e., the dependence of the frequency of autonomous oscillators on the input amplitude, and the chronaxia-rheobase function (Fig. 2); the response of the network to spatial heterogeneity in input amplitude), and basic network behavior (such as the dependence of synchrony on network connectivity and the dependence of the average frequency of the synchronized oscillation on the input amplitude) could be investigated.

This very first part of the study covered the reproduction of physiological data underlying the work of Wang and Buzsáki (1996). For example, we found that, as in their work, single disconnected model neurons were able to generate periodic action potentials over a wide frequency range (0–300 Hz; Fig. 2, left), which is a salient characteristic of hippocampal interneurons.

3.2 Spatially homogeneous, time-periodic stimulus current

By adding more complexity to the model we could study further properties of the network behavior. So far we had only investigated an isolated population of hippocampal interneurons. One way to expand the scope of the model was to take into account its interactions with

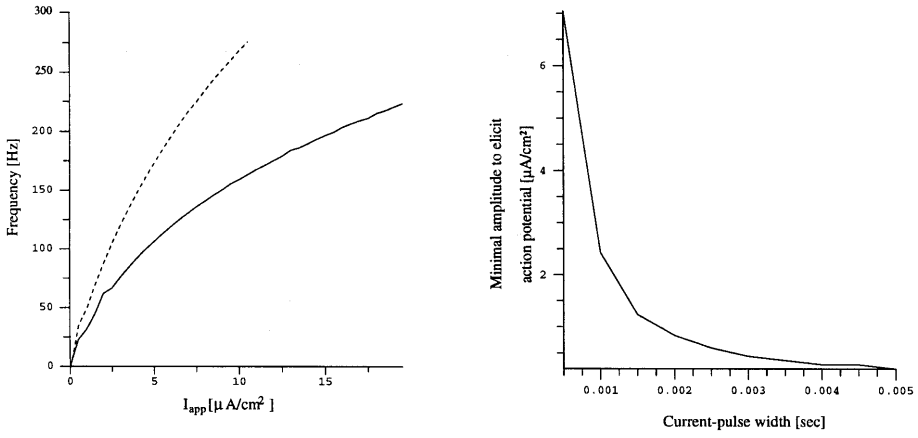

Fig. 2. *Left*: Isolated single-cell (*dashed line*) and network (*solid line*) oscillations in response to constant current injection. As a consequence of synaptic inhibition, the eigen-frequency of the system is smaller if neurons are coupled by inhibitory synapses. *Right*: Chronaxia-rheobase curve (the minimum current pulse amplitude that generates an action potential, as a function of pulse width) of the model interneuron. Rheobase was at 0.2 μA/cm^2

other neural populations. Obviously, it could have been done by defining other types of neurons, building other networks, and connecting them together. This, however, would have required large computational resources and long simulation times. Our strategy was to lump these inter-populational interactions into a single periodic stimulus current. Although the simulations were performed with purely sinusoidal input currents, similar results could be obtained with stimuli containing multiple Fourier components, such as square waveform input (data not shown).

Each neuron received an applied current I_{app}. For the single cell simulations (Sect. 3.1) this current was interpreted as the current injected into a cell through an electrode when measuring the cell's characteristic properties (Hodgkin and Huxley 1952). In the case of a network this interpretation was changed: the current $I_{app} = I_{DC}$ represented the integrated effect of all the excitatory inputs received by a certain neuron (Freund and Antal 1988; McCormick 1992). Using constant excitation presumed no knowledge about this input and was certainly not a realistic way of modeling short-range interactions in neural populations.

Anatomical and physiological experiments suggested that using temporally periodic excitation, rather than a constant stimulus, would be more plausible physiologically. Therefore a sinusoidal pattern generator was used, which supplied each cell with the same current (see also Sect. 2.3); i.e., the amplitude of the input was the same at a given time to all cells, and this amplitude changed in time as a sinusoidal function that was always set to be positive, meaning that current always flowed into the cells. Perforant path-evoked activities at the target cells are excitatory postsynaptic potentials. The perforant path delivers spike trains through numerous fibers to both interneurons and pyramidal cells. Thus periodic input currents in the model represented an integrated effect of these excitatory postsynaptic currents.

When the frequency of the stimulus current was the eigen-frequency of the network or a frequency close to it, the network was able to oscillate exactly with the same frequency (Fig. 3A and Fig. 4). This phenomenon was the result of resonance, as it was also characterized by a drop in the standard deviation of average cell frequencies ($\sigma_{\overline{f_{net}}}$), to near zero (Fig. 3B). Our investigations also showed that the DC component of the input current (I_{DC}) determined the eigen-frequency of the network (Fig. 3A), while the amplitude of the AC component (I_{AC}) was responsible for the width of the interval where our network worked as an identity operator, copying the frequency of the input to the output (Fig. 5).

Instantaneous frequencies (see Sect. 2.4) were found to change periodically and be phase-locked in time, thereby introducing a super-periodicity to the system (Fig. 6A). This behavior was significant when the stimulus frequency was far from the eigen-frequency of the

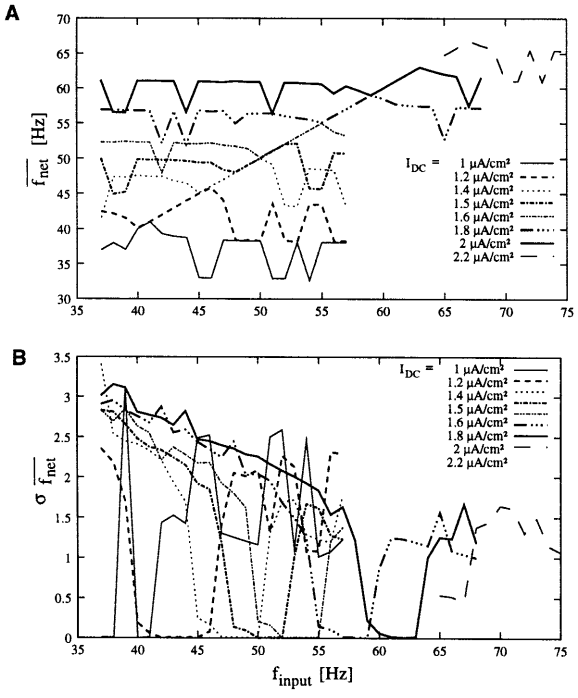

Fig. 3. Network resonance to periodic stimulation. Average network frequency (**A**) and standard deviation of average cell frequencies (**B**), as a function of the frequency (f_{input}) of a sinusoid current injection superimposed on different levels of constant current injection (I_{DC}), with $I_{AC}/I_{DC} = 0.3$ (see text for details). Resonance occurred where the output of the system followed the frequency of periodic perturbation, so the relation $f_{out}(f_{in}) = f_{in}$ was established and minimum deviation of individual cell frequencies was also achieved. Each line represents the average of three simulations

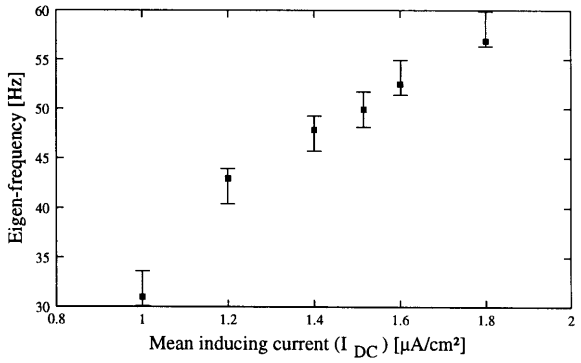

Fig. 4. Eigen-frequencies of the network as a function of mean stimulus current (I_{DC}). The average network frequency in response to constant current injection (*black rectangles*; see Fig. 2) was always within the interval where maximal network resonance occurred (*error bars*; see Fig. 3) in response to periodic stimulation ($I_{AC}/I_{DC} = 0.3$)

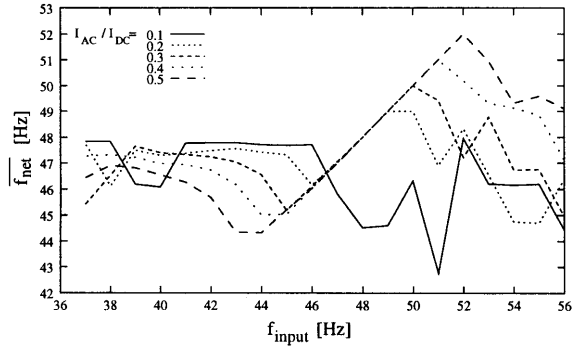

Fig. 5. Effect of a periodic perturbating current amplitude (I_{AC}) on average frequencies of the network ($\overline{f_{net}}$). With increasing relative amplitude of the periodic stimulus current (I_{AC}/I_{DC}; $I_{DC} = 1.4\ \mu A/cm^2$), network resonance occurred over a wider range of f_{input}. I_{AC} only influenced the size of this regime of linear input–output frequency correlation. Each line represents the average of three simulations

network. In the interval where the frequency input–output curve was linear, this pattern was not observed since the instantaneous frequencies were constant in time, i.e., firing rates of neurons did not change (Fig. 6A and Fig. 3B). It is the subject of further investigations as to how this periodic nature of the instantaneous frequency is controlled by the frequency of the input current.

An important property of the synchronization of the network was the time interval in which the network – starting from random initial conditions – reached a certain level of synchrony (Fig. 6B). Coherence in the network was measured by the time-dependent $\kappa^{\tau,T'}$ function defined in Sect. 2.4. We examined how properties of the stimulus current influenced the time needed for the synchrony to reach a value of 0.5. We found that, as a function of the frequency of the input current, this time had no typical behavior, but both κ^{τ} and the integral of $\kappa^{\tau,T'}$ (normalized by the simulation time, to make it a useful measure) showed a clear-cut maximum around the eigen-frequency of the network (Fig. 7). This meant that the time needed to reach a certain level of

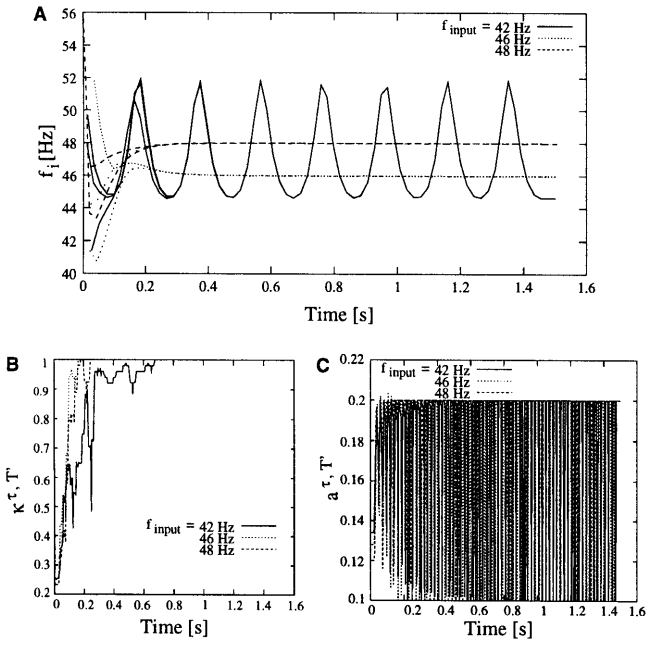

Fig. 6. Time courses of the instantaneous frequencies of three randomly chosen cells per simulation (**A**) in response to different input current frequencies (f_{input}). When f_{input} was in the resonance regime (*dashed* and *dotted lines*; see also Fig. 4), instantaneous frequencies remained constant, converging at the average network frequency. However, cells fired with oscillating frequencies when stimulated by a current of non-resonating frequency (*solid lines*). In all cases, cells become fully synchronized within a few hundred milliseconds (**B**). Network activity (**C**) also showed rapid saturation. Simulation parameters were $I_{AC}/I_{DC} = 0.3$ and $I_{DC} = 1.4\ \mu A/cm^2$

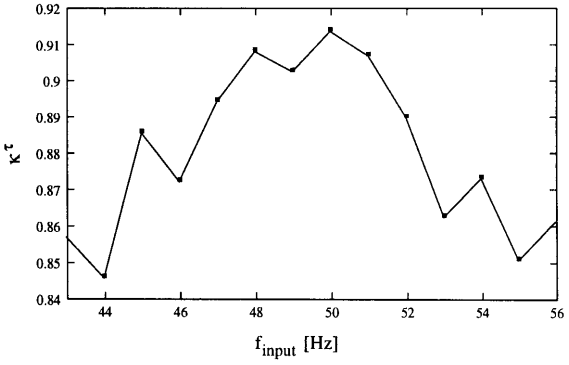

Fig. 7. Enhancement of network synchrony at input frequencies (f_{input}) near the eigen-frequency. Vertical axis gives κ^{τ} values. As in most cases $\kappa^{\tau,T'}$ reached approximately unity, this measure depended primarily on the time needed to reach full synchrony: the later the network synchronized the smaller the measure was. A significant increase in the neighborhood of the eigen-frequency indicates that oscillations induced in this range are more stable. Averages of thirty simulations are shown (*points*) for each parameter set ($I_{AC}/I_{DC} = 0.3$ and $I_{DC} = 1.4\ \mu A/cm^2$)

synchrony depended on the actual frequency of the network. As this frequency was determined mainly by the mean amplitude of the input current, i.e., of the input from the septum and the entorhinal cortex, these inputs regulated the transient time interval.

3.3 Spatially inhomogeneous, time-periodic stimulus current

The assumption that every cell receives the same input is only plausible when the propagation of the input signal is sufficiently fast compared to the characteristic cycle length of the oscillation. It is known that axonal conduction is slow, of order 1 mm/ms (~0.5 mm/ms in the Schaffer collaterals – Andersen et al. 1978), and a similar value can be expected in the perforant path as well. As coherent gamma oscillations occur over relatively large distances (e.g., over a 2-mm range along the longitudinal axis of the hippocampus – Bragin et al. 1995), phase lags greater than 1 ms may evolve in afferent fibers innervating different parts of this area, which is not negligible compared to the approximate 20 ms cycle of the oscillation. Thus the previously supposed zero time delay should be changed to achieve a more realistic scenario.

Therefore, a random term was added to the phase of the periodic input of each cell, mimicking the effect of axonal delays in afferent fibers of different length. This way, in spite of the fact that our model was single-compartmental – neglecting spatial extension – and that afferent fibers were not explicitly modelled, it was still possible to consider inhomogeneities caused by temporal differences. Similar temporal differences can arise from different axon fiber diameters. Signal propagation delays were not taken into account due to the short distances between interneurons. Two types of random term were studied: phase was either dispersed over the complete 0–360° interval (with a uniform distribution), or it was restricted to a Gaussian distribution of given standard deviation (σ_{ph}; see also Sect. 2.3).

With complete phase dispersion, simulations showed that the network resonated when stimulated near its eigen-frequency. As in the case of spatially homogeneous input, individual cells showed periodic oscillations in their instantaneous frequency, but waveforms were more complex in this case, and cells were not phase locked to each other; therefore, network synchrony could only reach a lower level (data not shown).

When phase dispersion of the stimulus current was restricted and its frequency was close to the eigen-frequency, the instantaneous frequency of cells behaved as if the phases of their stimuli had been identical. However, away from the eigen-frequency this stability of instantaneous frequencies diminished. While one instantaneous frequency function was practically sufficient to describe all cells during spatially homogeneous stimuli (as the cells were phase locked), with complete phase dispersion each instantaneous frequency function was characterized by a different time course. On the other hand, when phase dispersion was incomplete, cells could be divided to two subpopulations (as a compromise between the two extremes): one decreasing and the other increasing its firing rate between short periods of equal firing frequencies (Fig. 8A and 8B, upper panel, dotted

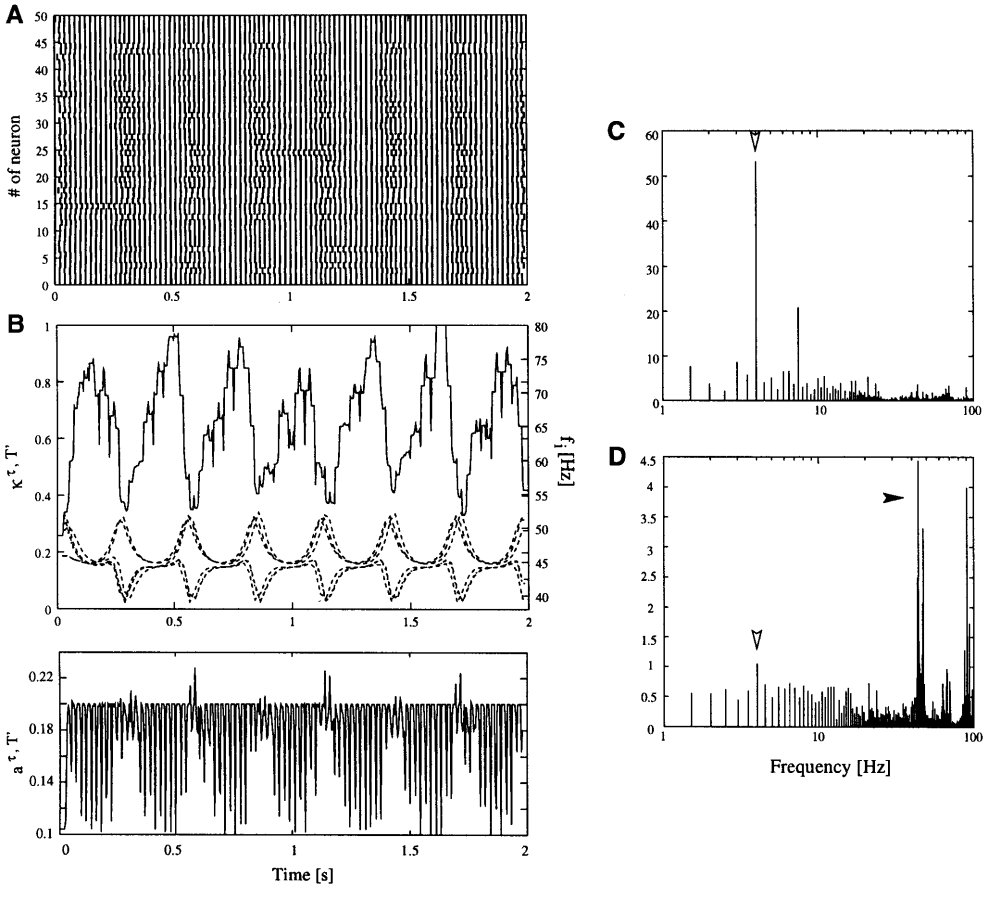

Fig. 8A–D. Network behavior in response to spatially phase-inhomogeneous periodic input. **A** Raster diagram of the network. Periodic synchronization and desynchronization of cells is apparent. **B** Oscillations in instantaneous frequency of five randomly chosen cells (f_i, *dashed lines*), network coherence ($\kappa^{\tau,T'}$, *solid line*), and network activity ($a^{\tau,T'}$, *below*) were synchronous and phase locked. **C** Power spectrum of $\kappa^{\tau,T'}$, showing a pronounced peak around 4 Hz (f_Θ, *empty arrowhead*). **D** Power spectrum of $a^{\tau,T'}$ with a primary peak around 40 Hz ($\overline{f_{net}}$) and a secondary peak at f_Θ (*filled* and *empty arrowheads*, respectively). Simulation parameters were $I_{AC}/I_{DC} = 0.3$, $I_{DC} = 1.4\ \mu A/cm^2$, $f_{input} = 43.3$ Hz and $\sigma_{ph} = 25°$

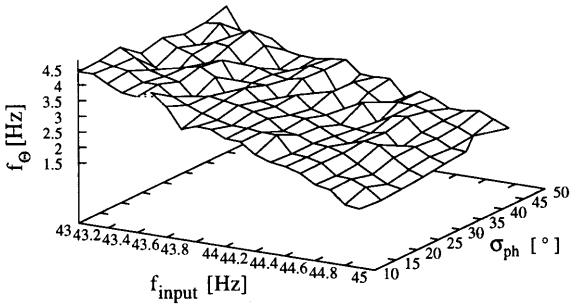

Fig. 9. Robustness of the oscillation in network synchrony. The frequency of the network oscillation (f_Θ) was less sensitive to phase heterogeneity (σ_{ph}) than to frequency (f_{input}) of the input. As the input frequency approached the eigen-frequency of the network (48 Hz at $I_{AC}/I_{DC} = 0.3$ and $I_{DC} = 1.4\ \mu A/cm^2$), f_Θ decreased

lines). Thus, synchrony evolved gradually when the firing rate was uniform over the network, and broke down as the difference grew between the frequencies of the two subpopulations. Together with the periodic changes in the instantaneous frequencies, a superimposed periodicity appeared both in the synchrony measure (Fig. 8B, upper panel, solid line), and in overall network activity (Fig. 8B, lower panel). This superimposed oscillation was present over a wide range of excitation frequencies, from 42.8 Hz to 44.9 Hz, and its frequency was 2–5 Hz (Fig. 8C,D and Fig. 9), just in the theta frequency domain.

The mechanism of this theta modulation was also investigated. There was a clear correlation between the phase of the input to a cell and its average firing rate (data not shown). Average firing rate was a useful parameter, as it indicated the subpopulation (accelerating or decelerating) to which the cell belonged. The amplitude of the instantaneous frequency oscillation had a critical role in determining the frequency of the theta oscillation. Theta oscillation was realized by the two distinct subpopulations, and the characteristic instantaneous frequency functions of these neuron groups changed periodically in anti-phase, in the sense that one group reached its maximum when the other reached its minimum. After the network become de-synchronized, it could only become synchronized again if the faster group had an advantage of a complete (gamma) cycle over the slower group. Thus the difference $\int_{T_\Theta}(f^F_{inst}(t) - f^S_{inst}(t))dt$, with F and S denoting a faster and a slower neuron, respectively, and T_Θ being the length of a theta cycle, had to be 2π. Furthermore, if phase dispersion was greater, deflection between the two subpopulations become greater and so a shorter interval was sufficient for the accelerating group to realize a complete gamma cycle advantage over the decelerating group. Thus theta cycles become shorter (the theta frequency increased) with increasing phase dispersion, as can be seen in Fig. 9. Although some aspects of this theta oscillation are not clearly understood (e.g., the negative correlation between theta frequency and input frequency is the subject of further investigation), this mechanism seems to be fairly robust over a wide range of input parameters. That is, it can be accepted as a biologically realistic mechanism for intrinsic theta oscillation generation in the hippocampus.

4 Discussion

Wang and Buzsáki (1996) showed that a randomly interconnected, inhibitory interneuron network was able to produce emergent synchronized oscillations in the gamma frequency band. By using the same model framework: (1) we have demonstrated that this network exhibits robust resonance when the stimulus frequency is close to the eigen-frequency of the network; and (2) considering the finite velocity of neural information transfer and the possible phase deviation of the stimulus, we also predict that a local network of CA3 interneurons is able to generate gamma-related theta oscillations. These predictions could be tested by making simultaneous paired recordings of oscillating interneurons.

There is a still an on-going debate about the neuroanatomical substrate of long-term synchronized neural oscillations. It is most likely that the mechanisms underlying such phenomena are manifold and cellular, local circuit and system levels contribute in different proportions to the net effect. Analysis of the interdependence of multiple hippocampal theta generators is a hot issue (Kocsis et al. 1999). Entorhinal cortex-mediated and intrahippocampal theta oscillators seem to be relatively independent, while theta signals from hippocampal fissure and CA1 *stratum oriens* are tightly coupled. Our model predicts that the emergent signal of an inhibitory interneuron network may control the membrane potential oscillations of principal cells during theta waves.

Theta-frequency periodic membrane potential oscillations of pyramidal cells are thought to be a result of the interplay between somatic inhibition and dendritic excitation (Kocsis et al. 1999). Previous work proposed that somatic inhibition arises from the septum (Buzsáki et al. 1983; Freund and Antal 1988) and is mediated by an inhibitory interneuron network to the somata of pyramidal cells (Fujita and Sato 1964; Ylinen et al. 1995; Tóth et al. 1997), while dendritic excitation originates from the entorhinal cortex and propagates through the perforant path (Mitchell et al. 1982; Alonso and Garcia-Austt 1987; Chrobak and Buzsáki 1998). However, using this model it is hard to see how the somatic and distal dendritic dipoles are coordinated to produce coherent signals. To resolve this point, previous theories have proposed that the septum is responsible for synchronous theta oscillations both in the entorhinal cortex and in the hippocampus, with septal neurons being well coordinated to produce a coherent rhythm. Contrary to this, septal neurons – both in anesthetized and awake animals – have been reported to discharge at any phase of a theta cycle (Stewart and Fox 1989, 1990). Therefore, the septum may not be the ultimate source of hippocampal theta rhythms.

Based on our modelling results, we propose the following alternative mechanism for generating gamma-related theta oscillations. The perforant path terminates

on interneurons (Buzsáki et al. 1987; Bragin et al. 1995) as well as on the dendritic tree of pyramidal cells, and delivers signals with characteristic frequencies in the gamma and theta bands. Electrophysiological experiments have shown that principal neurons of CA1 are resonant to theta-frequency excitation (Leung and Yu 1998), while in our model network interneurons selected a characteristic frequency in the gamma band. This gamma modulation invading the interneuron network through the perforant path is an appropriate substrate for the spatially inhomogeneous time-periodic stimulus that was neccessary to evoke theta oscillations in our network. Given these conditions, an intrahippocampal interneuron network appears to be a plausible candidate for the source of theta-modulated gamma oscillations in the hippocampus.

Appendix

$$C_{\mathrm{m}}\frac{\mathrm{d}V}{\mathrm{d}t} = -I_{\mathrm{Na}} - I_{\mathrm{K}} - I_{\mathrm{L}} - I_{\mathrm{syn}} + I_{\mathrm{app}} \tag{A1}$$

$$I_{\mathrm{L}} = g_{\mathrm{L}}(V - E_{\mathrm{L}}) \tag{A2}$$

$$I_{\mathrm{Na}} = g_{\mathrm{Na}} m_{\infty}^{3} h (V - E_{\mathrm{Na}}) \tag{A3}$$

$$m_{\infty} = \frac{\alpha_m}{\alpha_m - \beta_m} \tag{A4a}$$

$$\alpha_m = \frac{-0.1(V+35)}{\exp(-0.1(V+35)) - 1} \tag{A4b}$$

$$\beta_m = 4\exp\left(\frac{-V+60}{18}\right) \tag{A4c}$$

$$\frac{\mathrm{d}h}{\mathrm{d}t} = \phi(\alpha_h(1-h) - \beta_h h) \tag{A5a}$$

$$\alpha_h = 0.07\exp\left(\frac{-(V+58)}{20}\right) \tag{A5b}$$

$$\beta_h = \frac{1}{\exp(-0.1(V+28)) + 1} \tag{A5c}$$

$$I_{\mathrm{K}} = g_{\mathrm{K}} n^{4} (V - E_{\mathrm{K}}) \tag{A6}$$

$$\frac{\mathrm{d}n}{\mathrm{d}t} = \phi(\alpha_n(1-n) - \beta_n n) \tag{A7a}$$

$$\alpha_n = \frac{-0.1(V+34)}{\exp(-0.1(V+34)) - 1} \tag{A7b}$$

$$\beta_n = 0.125\exp\left(\frac{-(V+44)}{80}\right) \tag{A7c}$$

$$I_{\mathrm{syn}} = g_{\mathrm{syn}} s\left(V - E_{\mathrm{syn}}\right) \tag{A8}$$

$$\frac{\mathrm{d}s}{\mathrm{d}t} = \alpha F\left(V_{\mathrm{pre}}\right)(1-s) - \beta s \tag{A9}$$

$$F\left(V_{\mathrm{pre}}\right) = \frac{1}{1 + \exp\left(-\frac{V_{\mathrm{pre}} - \Theta_{\mathrm{syn}}}{2}\right)} \tag{A10}$$

Acknowledgements. This work was supported by the National Science Research Council (OTKA T 025500), and by the agreement between the DAAD and the Hungarian Fellowship Committee.

References

Alonso A, Garcia-Austt E (1987) Neuronal sources of the theta rhythm in the entorhinal cortex of the rat. II. Phase relations relations between unit discharges and theta field potentials. Exp Brain Res 67: 502–509

Andersen P, Silfvenius H, Sundberg S, Sveen O, Wigström H (1978) Functional characteristics of unmyelinated fibres in the hippocampal cortex. Brain Res 144: 11–18

Bragin A, Jandó G, Nádasdy Z, Hetke J, Wise K, Buzsáki G (1995) Gamma (40–100 Hz) Oscillation in the hippocampus of the behaving rat. J Neurosci 15: 47–60

Buzsáki G (1998) Memory consolidation during sleep: a neurophysiological perspective. J Sleep Res 1: 17–23

Buzsáki G, Gage FH, Czopf J, Bjorklund A (1987) Restoration of a rhythmic slow activity (theta) in the subcortically denervated hippocampus by fetal CNS transplants. Brain Res 400: 334–347

Buzsáki G, Horváth Z, Urioste R, Hetke T, Wise K (1992) High-frequency network oscillation in the hippocampus. Science 256: 1025–1027

Buzsáki G, Leung LS, Vanderwolf CH (1983) Cellular bases of hippocampal EEG in the behaving rat. Brain Res Rev 6: 139–171

Chapman CA, Lacille J-C (1999) Intrinsic theta-frequency membrane potential oscillation in hippocampal CA1 interneurons of stratum lacunosum-moleculare. J Neurophysiol 81: 1296–1307

Chrobak JJ, Buzsáki G (1998) Gamma oscillation in the entorhinal cortex of the freely behaving rat. J Neurosci 18: 388–398

Fox SE, Ranck Jr JB (1986) Hippocampal theta rhythm and the firing of neurons in walking and urethane anesthetized rats. Exp Brain Res 62: 495–508

Freund TF, Antal M (1988) GABA-containing neurons in the septum control inhibitory interneurons in the hippocampus. Nautre 336: 170–173

Fujita Y, Sato T (1964) Intracellular record from hippocampal pyramidal cells in rabbit during theta rhythmic activity. J Neurophysiol 27: 1011–1025

Gray CM, König P, Engel AK, Singer W (1989) Stimulus-specific neuronal oscillations in cat visual cortex exhibit inter-columnar synchronization which reflects global stimulus property. Nature 338: 334–337

Hodgkin AL, Huxley AF (1952) A quantitative description of membrane current and its application to conduction and excitation in nerve. J Physiol (Lond) 117: 500–544

Jensen O, Lisman JE (1996) Theta/gamma networks with slow NMDA channels learn sequences and encode episodic memory: role of NMDA channels in recall. Learn Mem 3: 264–278

Katona I, Acsády L, Freund T (1999) Postsynaptic targets of somatostatin-immunoreactive interneurons in the rat hippocampus. Neuroscience 88: 37–55

Kocsis B, Bragin A, Buzsáki G (1999) Interdependence of multiple theta generators in the hippocampus: a partial coherence analysis. J Neurosci 19: 6200–6212

Léránth C, Frotscher M (1987) Cholinergic innervation of hippocampal GAD- and somatostatin-immunoreactive commissural neurons. J Comp Neurol 261: 33–47

Leung LS, Lopes da Silva FH, Wadman WJ (1982) Spectral characteristics of the hippocampal EEG in the freely moving rat. Electroencephalogr Clin Neurophysiol 54: 203–219

Leung LS, Yim CY (1991) Intrinsic membrane potential oscillations in hippocampal neurons in vitro. Brain Res 553: 261–274

Leung LS, Yu HW (1998) Theta frequency resonance in hippocampal CA1 neurons in vitro demonstrated by sinusoidal current injection. J Neurophysiol 79: 1592–1596

McCormick DA (1992) Neurotransmitter action in the talamus and cerebral cortex and their role in neuromodulation of thalamocortical activity. Prog Neurobiol 39: 337–388

Mitchell SJ, Ranck Jr JB, Steward O, Olton DS (1982) Medial septal area lesions disrupt theta rhythm and cholinergic staining in medial entorhinal cortex and produce impaired radial arm mase behaviour in rat. J Neurosci 2: 292–302

O'Keefe J, Recce ML (1993) Phase relationship between hippocampal place units and the EEG theta rhythm. Hippocampus 3: 317–330

Petsche H, Stumpf C, Gogolak G (1962) The significance of the rabbit's septum as a relay station between the mid-brain and the hippocampus. I. The control of hippocampal arousal activity by the septum cells. Electroencephalogr Clin Neurophysiol 14: 202–211

Skaggs WE, McNaughton BL, Wilson MA, Barnes CA (1996) Theta phase precession in hippocampal neuronal populations and the compression of temproral sequences. Hippocampus 6: 149–172

Stewart M, Fox SE (1989) Firing relations of medial septal neurons to the hippocampal theta rhythm in urethane anesthetized rats. Exp Brain Res 77: 507–516

Stewart M, Fox SE (1990) Do septal neurons pace the hippocampal theta rhythm? Trends Neurosci 13: 163–168

Strata F (1998) Intrinsic oscillations in CA3 pyramids: physiological relevance to theta rhythm generation. Hippocampus 8: 666–679

Tóth K, Freund TF, Miles R (1997) Disinhibition of rat hippocampal pyramidal cells by GABAergic afferents from the septum. J Physiol (Lond) 500: 463–474

Traub RD, Jefferys JGR, Whittington MA (1999a) Fast Oscillations in Cortical Circuits. The MIT Press, Cambridge, Mass.

Traub RD, Whittington MA, Buhl EH, Jefferys JGR, Faulkner HJ (1999b) On the mechanism of the $\gamma \rightarrow \beta$ frequency shift in neuronal oscillations induced in rat hippocampal slices by tetanic stimulation. J Neurosci 19: 1088–1105

Vanderwolf CH (1969) Hippocampal electrical activity and voluntary movement in the rat. Electroencephalogr Clin Neurophysiol 26: 407–418

Wang XJ (1993) Ionic basis for intrinsic 40 Hz neural oscillations Neuroreport 5: 221–224

Wang XJ, Buzsáki G (1996) Gamma oscillation by synaptic inhibition in a hippocampal interneuronal network model. J Neurosci 6: 6402–6413

Whittington MA, Traub RD, Jefferys JGR (1995) Synchronized oscillations in interneuron networks driven by metabotropic glutamate receptor activation. Nature 373: 612–615

Ylinen A, Soltész I, Bragin A, Pentonnen M, Sík A, Buzsáki G (1995) Intracellular correlates of hippocampal theta rhythm in identified pyramidal cells, granule cells, and basket cells. Hippocampus 5: 78–90